

Reconstructing a metazoan genetic pathway with transcriptome-wide epistasis measurements

David Angeles-Albores^{a, b, 1}, Carmie Puckett Robinson^{a, b, c, 1}, Brian A. Williams^a, Barbara J. Wold^a, and Paul W. Sternberg^{a, b}

^aDivision of Biology and Biological Engineering, Caltech, Pasadena, CA, 91125, USA; ^bHoward Hughes Medical Institute, Caltech, Pasadena, CA, 91125, USA; ^cDepartment of Neurology, Keck School of Medicine, University of Southern California, Los Angeles, California, 90033, USA

This manuscript was compiled on September 27, 2017

RNA-seq is commonly used to identify genetic modules that respond to perturbations. In single cells, transcriptomes have been used as phenotypes, but this concept has not been applied to whole-organism RNA-seq. Also, quantifying and interpreting epistatic effects using expression profiles remains a challenge. We developed a single coefficient to quantify transcriptome-wide epistasis that reflects the underlying interactions and which can be interpreted intuitively. To demonstrate our approach, we sequenced four single and two double mutants of *Caenorhabditis elegans*. From these mutants, we reconstructed the known hypoxia pathway. In addition, we uncovered a class of 56 genes with *hif-1*-dependent expression which have opposite changes in expression in mutants of two genes which cooperate to negatively regulate HIF-1 abundance; however, the double mutant of these genes exhibits suppression epistasis. This class violates the classical model of HIF-1 regulation, but can be explained by postulating a role of hydroxylated HIF-1 in transcriptional control.

Epistasis | Genetic Interaction | Transcriptome | Hypoxia

Genetic analysis of molecular pathways has traditionally been performed through epistatic analysis. If the mutants of two distinct genes have a quantifiable phenotype, and the double mutant has a phenotype that is not the sum of the phenotypes of the single mutants, this non-additivity is referred to as generalized epistasis, and indicates that these genes interact functionally. Such interactions can occur at the biochemical level between their products or as a consequence of their functions (1). Epistasis analysis remains a cornerstone of genetics today (2).

Recently, biological studies have shifted in focus from studying single genes to studying all genes in parallel. In particular, RNA-seq (3) enables biologists to identify genes that change expression in response to a perturbation. RNA-seq has been used to identify genetic modules involved in a variety of processes, such as in the *Caenorhabditis elegans* linker cell migration (4), planarian stem cell maintenance (5, 6). The role of transcriptional profiling has been restricted to target gene identification, and so far there are only a few examples where transcriptomes have been used to generate quantitative genetic models of any kind. In quantitative genetics, eQTL studies have established the power of transcriptomes for genetic mapping (7–10). Genetic pathway analysis via epistasis has been performed in *Saccharomyces cerevisiae* (11, 12) and in *Dicystostelium discoideum* (13). Recently, Dixit *et al* described a protocol for epistasis analysis in dendritic and K562 cells using single-cell RNA-seq (14). Epistasis analysis of single cells or single-celled organisms is popular because of the concern that whole-organism sequencing will mix information from multiple cell types, preventing the accurate reconstruction of genetic interactions. Using whole-organism transcriptome profiling,

we have recently identified a new developmental state of *C. elegans* caused by loss of a single cell type (sperm cells) (15), which suggests that whole-organism transcriptome profiling contains sufficient information for epistatic analysis. To investigate the ability of whole-organism transcriptomes to serve as quantitative phenotypes for epistatic analysis in metazoans, we sequenced the transcriptomes of four well-characterized loss-of-function mutants in the *C. elegans* hypoxia pathway (16–19).

Metazoans depend on the presence of oxygen in sufficient concentrations to support aerobic metabolism. Hypoxia inducible factors (HIFs) are an important group of oxygen-responsive genes that are highly conserved in metazoans (20). A common mechanism for hypoxia-response induction is heterodimerization between a HIF α and a HIF β subunit; the heterodimer then initiates transcription of target genes (21). The number and complexity of HIFs varies throughout metazoans. In the roundworm *C. elegans* there is a single HIF α gene, *hif-1* (19), and a single HIF β gene, *ahr-1* (22).

Levels of HIF α proteins are tightly regulated. Under conditions of normoxia, HIF-1 α exists in the cytoplasm and partakes in a futile cycle of protein production and rapid degrada-

Significance Statement

Transcriptome profiling is a way to quickly and quantitatively measure gene expression level. There is widespread interest in using transcriptomic profiles as a phenotype for genetic analysis. However, a source of concern is that whole-animal transcriptomic profiles mix the expression signatures of multiple cellular states, which might make it hard to accurately reconstruct genetic interactions. Additionally, it has been difficult to measure epistasis, the signature of genetic interaction between two genes, using expression profiles. Here, we show that it is possible to accurately reconstruct genetic interactions between genes using whole-animal RNA sequencing, and we demonstrate a way to quantify epistasis transcriptome-wide. With the advent of genome engineering tools, mutants can be created quickly and easily in many organisms. As a result, phenotyping mutants is the rate-limiting step towards reconstructing genetic interaction networks. Our work potentially represents a solution to this problem because transcriptome profiling is sensitive to a broad variety of genetic perturbations.

DAA, CPR and PWS designed experiments. CPR and BAW performed all experiments. BJW provided resources. DAA developed computational methods and performed analysis. DAA, CPR and PWS wrote the paper.

The authors declare no conflict of interest.

¹ DAA and CPR contributed equally to this work.

²To whom correspondence should be addressed. E-mail: pws@caltech.edu

tion (23). In *C. elegans*, HIF-1 α is hydroxylated by a proline hydroxylase (EGL-9) (24). HIF-1 hydroxylation increases its binding affinity to Von Hippel-Lindau tumor suppressor 1 (VHL-1), which in turn allows ubiquitination of HIF-1 leading to its degradation. In *C. elegans*, EGL-9 activity is inhibited by binding of CYSL-1, a homolog of sulfhydrylases/cysteine synthases; and CYSL-1 activity is in turn inhibited by the putative transmembrane O-acyltransferase RHY-1, possibly by post-translational modifications to CYSL-1 (25) (see Fig. 1).

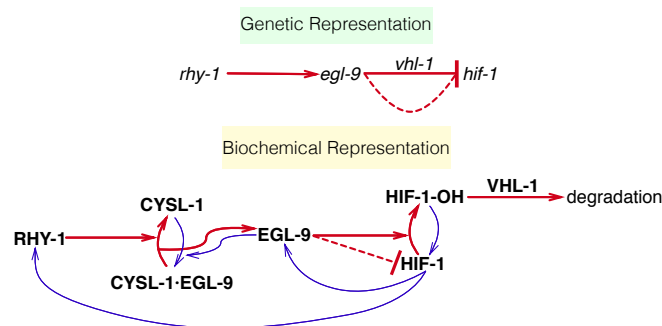


Fig. 1. Genetic and biochemical representation of the hypoxia pathway in *C. elegans*. Red arrows are arrows that lead to inhibition of HIF-1, and blue arrows are arrows that increase HIF-1 activity or are the result of HIF-1 activity. EGL-9 is known to exert VHL-1-dependent and independent repression on HIF-1 as shown in the genetic diagram. The VHL-1-independent repression of HIF-1 by EGL-9 is denoted by a dashed line and is not dependent on the hydroxylating activity of EGL-9. RHY-1 inhibits CYSL-1, which in turn inhibits EGL-9, but this interaction was abbreviated in the genetic diagram for clarity.

Our reconstruction of the hypoxia pathway in *C. elegans* shows that whole-animal transcriptome profiles can be used as phenotypes for genetic analysis and that epistasis, a hallmark of genetic interaction observed in double mutants, holds at the molecular systems level. We demonstrate that transcriptomes can aid in ordering genes in a pathway using only single mutants. We were able to identify genes that appear to be downstream of *vhl-1*, but not downstream of *hif-1*. Using a single set of transcriptome-wide measurements, we observed most of the known transcriptional effects of *hif-1* as well as novel effects not described before in *C. elegans*. Taken together, this analysis demonstrates that whole-animal RNA-seq is a fast and powerful method for genetic analyses in an area where phenotypic measurements are now the rate-limiting step.

Results

The hypoxia pathway controls thousands of genes in *C. elegans*. We selected four null single mutants within the hypoxia pathway for expression profiling: *egl-9(sa307)*, *rhy-1(ok1402)*, *vhl-1(ok161)*, *hif-1(ia4)*. We also sequenced the transcriptomes of two double mutants, *egl-9; vhl-1* and *egl-9 hif-1* as well as wild type (N2). Each genotype was sequenced in triplicate using mRNA extracted from 30 worms per sample at a depth of 15 million reads per sample, of which 7 million reads mapped to the *C. elegans* genome. All samples were analyzed only under normoxic conditions. We identified around 22,000 different isoforms per sample, which allowed us to measure differential expression of 18,344 isoforms across all replicates and genotypes (~70% of the protein coding isoforms in *C. elegans*; see Basic Statistics Notebook). We included in our analysis a *fog-2(q71)* mutant we have previously studied (15),

because *fog-2* is not reported to interact with the hypoxia pathway. We analyzed our data using a general linear model on logarithm-transformed counts. Changes in gene expression are reflected in the regression coefficient β , which is specific to each isoform within a genotype (excluding wild type, which is used as baseline). Statistical significance is achieved when the q -value of a β coefficient (p -values adjusted for multiple testing) are less than 0.1. Transcripts that are differentially expressed between the wild type and a given mutant have β values that are statistically significantly different from 0 (i.e. greater than 0 or less than 0). β coefficients are analogous to the logarithm of the fold-change between the mutant and the wild type. Larger magnitudes of β correspond to larger perturbations (see Fig. 2). When we refer to β coefficients and q -values, it will always be in reference to isoforms. However, we report the sizes of each gene set by the number of differentially expressed genes (DEGs), not isoforms, they contain. For the case of *C. elegans*, this difference is negligible since the great majority of protein-coding genes have a single isoform. We have opted for this method of referring to gene sets because it simplifies the language considerably. A complete version of the code used for this analysis with ample documentation, is available at <https://wormlabcaltech.github.io/mpsrq>.

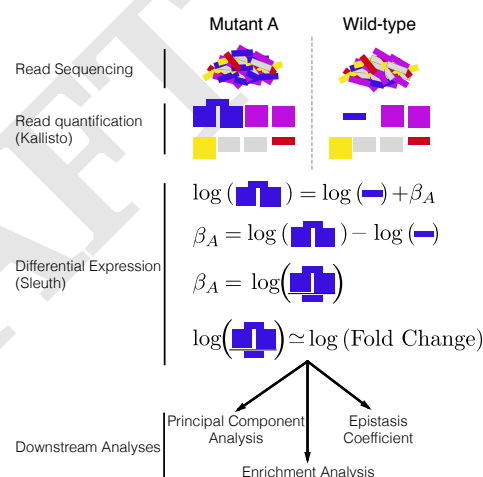


Fig. 2. Analysis workflow. After sequencing, reads are quantified using Kallisto. Bars show estimated counts for each isoform. Differential expression is calculated using Sleuth, which outputs one β coefficient per isoform per genotype. β coefficients are analogous to the natural logarithm of the fold-change relative to a wild type control. Downstream analyses are performed with β coefficients that are statistically significantly different from 0. q -values less than 0.1 are considered statistically different from 0.

Transcriptome profiling of the hypoxia pathway revealed that this pathway controls thousands of genes in *C. elegans* (see Table 1). The *egl-9(lf)* transcriptome showed differential expression of 2,549 genes. 3,005 genes were differentially expressed in *rhy-1(lf)* mutants. The *vhl-1(lf)* transcriptome showed considerably fewer DEGs (1,275), possibly because *vhl-1* is a weaker inhibitor of *hif-1* than *egl-9* (18). The *egl-9(lf);vhl-1(lf)* double mutant transcriptome showed 3,654 DEGs. The *hif-1(lf)* mutant showed a transcriptomic phenotype involving 1,075 genes. The *egl-9(lf) hif-1(lf)* double mutant showed a similar number of genes with altered expression (744 genes). We do not think that this transcriptional response is the due to transiently induced hypoxia during harvesting. If the wild type strain had become hypoxic,

then the *hif-1(lf)* genotype should show significantly lower levels of *nhr-57*, a marker that increases during hypoxia. We do not observe altered levels of *nhr-57* when comparing the wild type and *hif-1(lf)* mutant, nor between the wild type and *egl-9(lf)* *hif-1(lf)* double mutant. Finally, the *egl-9(lf)*, *vhl-1(lf)*, *rhy-1(lf)* and *egl-9(lf)*; *vhl-1(lf)* mutants did show altered *nhr-57* transcript levels (see [Quality Control Notebook](#)). We cannot rule out cumulative effects from loss of *hif-1* or strain-specific eQTLs present in the strain background.

Genotype	Differentially Expressed Genes
<i>egl-9(lf)</i>	2,549
<i>rhy-1(lf)</i>	3,005
<i>vhl-1(lf)</i>	1,275
<i>hif-1(lf)</i>	1,075
<i>egl-9(lf)</i> ; <i>vhl-1(lf)</i>	3,654
<i>egl-9(lf)</i> <i>hif-1(lf)</i>	744
<i>fog-2(lf)</i>	2,840

Table 1. Number of differentially expressed genes in each mutant strain with respect to the wild type (N2).

Principal Component Analysis visualizes epistatic relationships between genotypes. Principal component analysis (PCA) is used to identify relationships between high-dimensional data points (26). We used PCA to examine whether each genotype clustered in a biologically relevant manner. PCA identifies the vector that explains most of the variation in the data; this is called the first principal component. PCA can identify the first n components that explain more than 95% of the data variance. Clustering in these n dimensions can indicate biological relationships, although interpreting principal components can be difficult. In our analysis, the first principal component discriminated mutants that have constitutive high levels of HIF-1 from mutants that have no HIF-1, whereas the second component was able to discriminate between mutants within the hypoxia pathway and outside the hypoxia pathway (see Fig. 3; *fog-2* is not reported to act in the hypoxia pathway and acts as a negative control; see [Genetic Interactions Notebook](#)).

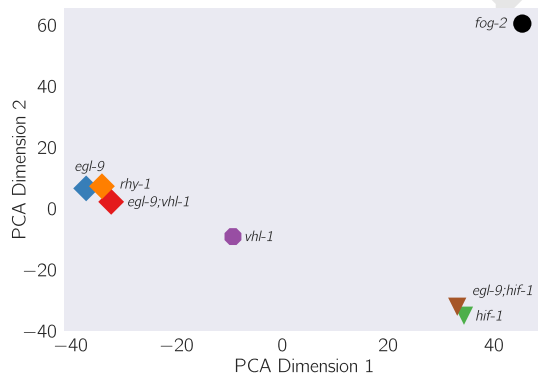


Fig. 3. Principal component analysis of various *C. elegans* mutants. Genotypes that have an constitutive hypoxia response (i.e. *egl-9(lf)*) cluster far from genotypes that do not have a hypoxic response (i.e. *hif-1(lf)*) along the first principal component. The second principal component separates genotypes that do not participate hypoxic response pathway.

Reconstruction of the hypoxia pathway from first genetic principles. To reconstruct a genetic pathway, we must assess whether two genes act on the same phenotype. If they do not act on the same phenotype (two mutations do not cause the same genes to become differentially expressed relative to wild type), these mutants are independent. Otherwise, we must measure whether these genes act additively or epistatically on the phenotype of interest; if there is epistasis we must measure whether it is positive or negative, in order to assess whether the epistatic relationship is a genetic suppression or a synthetic interaction. To allow coherent comparisons of different mutant transcriptomes (the phenotype we are studying here), we define the shared transcriptomic phenotype (STP) between two mutants as the shared set of genes or isoforms whose expression in both mutants are different from wild-type, regardless of the direction of change.

Genes in the hypoxia mutant act on the same transcriptional phenotype. All the hypoxia mutants had a significant STP: the fraction of differentially expressed genes that was shared between mutants ranged from a minimum of 10% shared between *hif-1(lf)* and *egl-9(lf)*; *vhl-1(lf)* to a maximum of 32% shared genes between *egl-9(lf)* and *egl-9(lf)*; *vhl-1(lf)*. For comparison, we also analyzed a previously published *fog-2(lf)* transcriptome (15). The *fog-2* gene is involved in masculinization of the *C. elegans* germline, which enables sperm formation, and is not known to be involved in the hypoxia pathway. The hypoxia pathway mutants and the *fog-2(lf)* mutant also had STPs (8.8%–14% genes).

Next, we performed pairwise correlations between all mutant pairs. We rank-transformed the β coefficients of each isoform between the STP of two mutants, and calculated lines of best fit using Bayesian regressions that are robust to outliers (see Fig 4). For mutants associated with the hypoxia pathway, these correlations have values higher than 0.9 with a tight distribution around the line of best fit. The correlations for mutants from the hypoxia pathway with the *fog-2(lf)* mutant were considerably weaker, with magnitudes between 0.6–0.85 and greater variance around the line of best fit. Although *hif-1* is known to be genetically repressed by *egl-9*, *rhy-1* and *vhl-1* (16, 17), all the correlations between mutants of these genes and *hif-1(lf)* were positive (see [Genetic Interactions Notebook](#)). We reasoned that this apparent contradiction could be due to either strain-specific eQTLs in our N2 background (an artifactual signal) or that it could reflect a previously unrecognized aspect of HIF-1 biology. This motivated us to look for genes that exhibited verifiable extreme patterns of anomalous behavior and led us to propose a new model of the hypoxia pathway (see Identification of non-classical epistatic interactions).

Transcriptome-wide epistasis. Ideally, any measurement of transcriptome-wide epistasis should conform to certain expectations. First, it should make use of the regression coefficients of as many genes as possible. Second, it should be summarizable in a single, well-defined number. Third, it should have an intuitive behavior, such that special values of the statistic have an unambiguous interpretation.

We found an approach that satisfies all of the above conditions and which can be graphed in an epistasis plot (see Fig 5) In an epistasis plot, the X-axis represents the expected β coefficient for given gene in a double mutant a^-b^- if a and

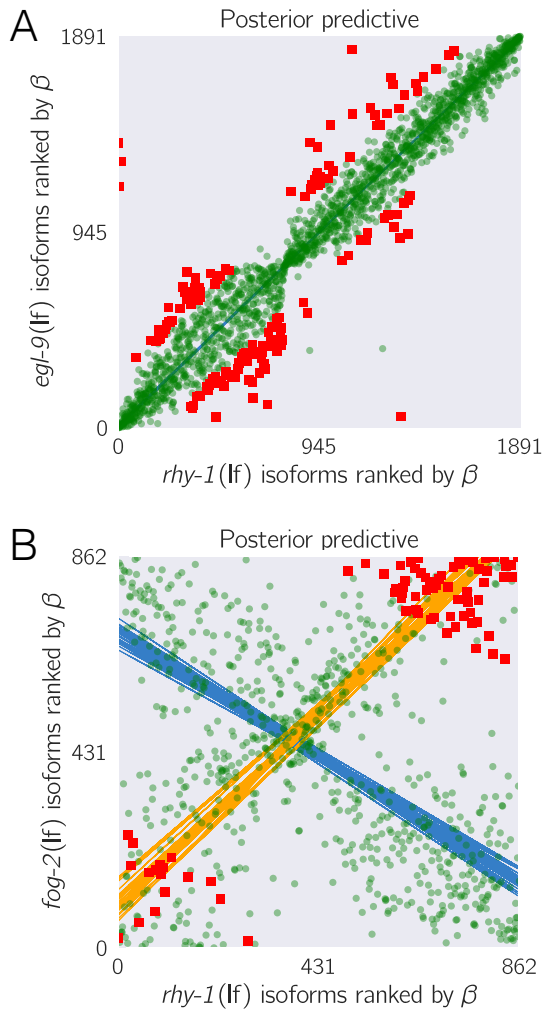


Fig. 4. Strong transcriptional correlations exist between genes that share positive regulatory connections. **A.** We identified isoforms that were differentially expressed in both *egl-9(lf)* and the *rhy-1(lf)* mutants, and ranked each isoform according to its β coefficient. We plotted the rank of each isoform in *rhy-1(lf)* versus the rank of the same isoform in the *egl-9(lf)* transcriptome. **B.** For comparison, we followed the same procedure with the *fog-2(lf)* and *rhy-1(lf)* transcriptomes. *fog-2(lf)* is not known to interact with the primary hypoxia pathway. Green, transparent points mark inliers to the primary regressions (blue lines); red squares mark outliers to the primary regressions. Orange lines show secondary regressions performed on the outliers.

b interact log-additively. In other words, each individual isoform's x-coordinate is the sum of the regression coefficients from the single mutants a^- and b^- . The Y-axis represents the deviations from the log-additive (null) model, and can be calculated as the difference between the predicted and the observed β coefficients. Only isoforms that are differentially expressed in all three genotypes are plotted. This attempts to ensure that the isoforms to be examined are regulated by both genes. These plots will generate specific patterns that can be described through linear regressions. The slope of these lines, to which we assign the mathematical notation $s(a, b)$, is the transcriptome-wide epistasis coefficient.

Transcriptome-wide epistasis coefficients can be understood intuitively for simple cases of genetic interactions if complete genetic nulls are used. If two genes act additively on the same set of differentially expressed isoforms then all the plotted points will fall along the line $y = 0$. If two genes act positively in an unbranched pathway, then all the mutants should have the same phenotype. It follows that data from this pathway will form line with slope equal to $-\frac{1}{2}$. On the other hand, in the limit of complete genetic inhibition of b by a in an unbranched pathway (i.e., a is in great excess over b , such that under the conditions measured b has no activity), the plots should show a line of best fit with slope equal to -1 . Genes that interact synthetically (i.e., through an OR-gate) will fall along lines with slopes > 0 . When there is epistasis of one gene over another, the points will fall along one of two possible slopes that must be determined empirically from the single mutant data. We can use both single mutant data to predict the distribution of slopes that results for the cases stated above. Thus, the transcriptome-wide epistasis coefficient integrates information from many different isoforms into a single number (see Fig. 5).

In our experiment, we studied two double mutants, *egl-9(lf) hif-1(lf)* and *egl-9(lf); vhl-1(lf)*. We wanted to understand how well an epistatic analysis based on transcriptome-wide coefficients agreed with the epistasis results reported in the literature, which were based on qPCR of single genes. Therefore, we performed orthogonal distance regression on the two gene combinations we studied (*egl-9* and *vhl-1*, and *egl-9* and *hif-1*) to determine the epistasis coefficient for each gene pair. Finally, although we could compute an epistasis coefficient from these factors, we would also like to know which gene is being suppressed in the double mutant. Since suppression means that the double mutant should have exactly the phenotype of one and only one mutant, we can simulate the double mutant by replacing the double mutant data with either of the two single mutants and matching the simulated result to the observed result. The result that most closely matches the real data will reveal which gene is being suppressed, which in turn allows us to order the genes along a pathway.

We measured the epistasis coefficient between *egl-9* and *vhl-1*, $s(egl-9 \ vhl-1) = -0.41$ (see Epistasis Notebook). Simulations using just the single mutant data showed that the double mutant exhibited the *egl-9(lf)* phenotype (see Fig. 5). We used Bayesian model selection to reject a linear pathway (odds ratio (OR) $> 10^{83}$), which leads us to conclude *egl-9* is upstream of *vhl-1* acting on a phenotype in a branched manner. We also measured epistasis between *egl-9* and *hif-1*, $s(egl-9, hif-1) = -0.80$, and we found that this behavior could be predicted by modeling *hif-1* downstream of *egl-9*. We also

rejected the null hypothesis that these two genes act in a positive linear pathway ($OR > 10^{93}$). Taken together, this leads us to conclude that *egl-9* strongly inhibits *hif-1*.

Epistasis between two genes can be predicted using an upstream component. Given our success in measuring epistasis coefficients, we wanted to know whether it would be possible to predict the epistasis coefficient between *egl-9* and *vhl-1* in the absence of the *egl-9(lf)* genotype. Since RHY-1 indirectly activates EGL-9, we reasoned that the *rhy-1(lf)* transcriptome should contain almost equivalent information to the *egl-9(lf)* transcriptome. Therefore, we generated predictions of the epistasis coefficient between *egl-9* and *vhl-1* by substituting in the *rhy-1(lf)* data, predicting $s(rhy - 1, vhl - 1) = -0.45$. Similarly, we used the *egl-9(lf); vhl-1(lf)* double mutant to measure the epistasis coefficient while replacing the *egl-9(lf)* dataset with the *rhy-1(lf)* dataset. We found that the epistasis coefficient using this substitution was -0.40 . This coefficient was different from -0.50 ($OR > 10^{62}$), reflecting the same qualitative conclusion that *vhl-1* represents a branch in the hypoxia pathway. We were able to obtain a close prediction of the epistasis coefficient for two mutants using the transcriptome of a related, upstream mutant.

Transcriptomic decorrelation can be used to infer functional distance. So far, we have shown that RNA-seq can accurately measure genetic interactions. However, genetic interactions do not require two gene products to interact biochemically, nor even to be physically close to each other. RNA-seq cannot measure physical interactions between genes, but we wondered whether expression profiling contains sufficient information to order genes along a pathway.

Single genes are often regulated by multiple independent sources. The connection between two nodes can in theory be characterized by the strength of the edges connecting them (the thickness of the edge); the sources that regulate both nodes (the fraction of inputs common to both nodes); and the genes that are regulated by both nodes (the fraction of outputs that are common to both nodes). In other words, we expected that expression profiles associated with a pathway would respond quantitatively to quantitative changes in activity of the pathway. Targeting a pathway at multiple points would lead to expression profile divergence as we compare nodes that are separated by more degrees of freedom, reflecting the flux in information between them.

We investigated this possibility by weighting the robust Bayesian regression between each pair of genotypes by the size of the shared transcriptomic phenotype of each pair divided by the total number of isoforms differentially expressed in either mutant ($N_{\text{Intersection}}/N_{\text{Union}}$). We plotted the weighted correlation of each gene pair, ordered by increasing functional distance (see Fig. 6). In every case, we see that the weighted correlation decreases monotonically due mainly, but not exclusively, to a smaller STP (see [Decorrelation Notebook](#)).

We believe that this result is not due to random noise or insufficiently deep sequencing. Instead, we propose a framework in which every gene is regulated by multiple different molecular species, which induces progressive decorrelation. This decorrelation in turn has two consequences. First, decorrelation within a pathway implies that two nodes may be almost independent of each other if the functional distance between them is large. Second, it may be possible to use decorrelation

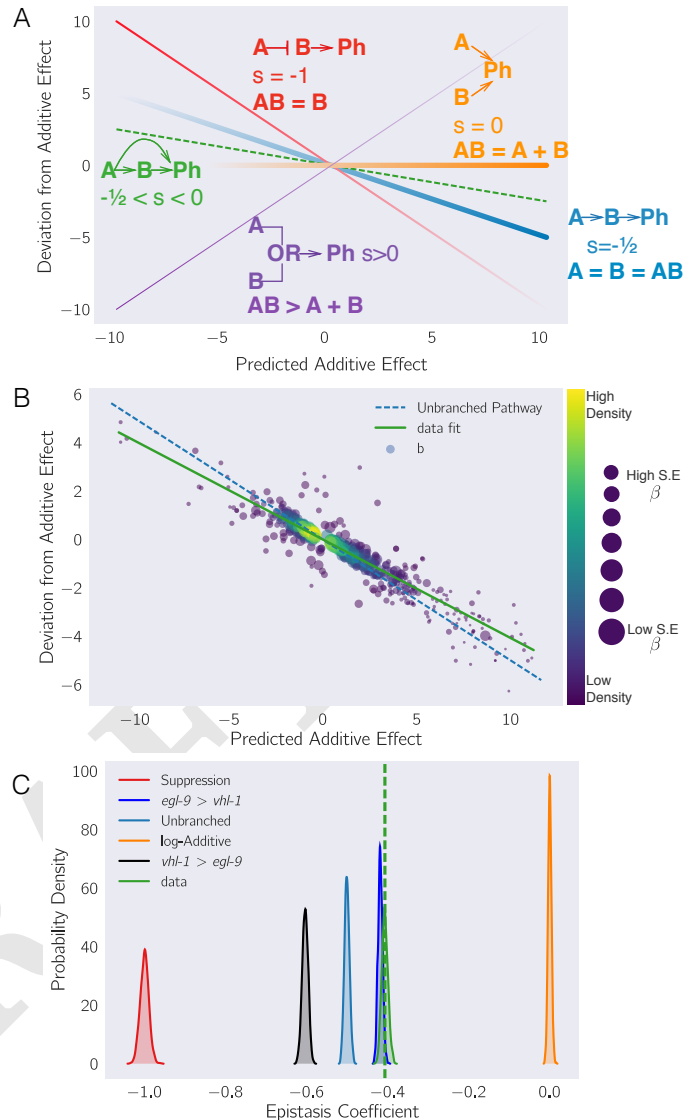


Fig. 5. (A) Schematic diagram of an epistasis plot. The X-axis on an epistasis plot is the expected coefficient for a double mutant under an log-additive model (null model). The Y-axis plots deviations from this model. Double mutants that deviate in a systematic manner from the null model exhibit transcriptome-wide epistasis (s). To measure s , we find the line of best fit and determine its slope. Genes that act log-additively on a phenotype (**Ph**) will have $s = 0$ (null hypothesis, orange line); whereas genes that act along an unbranched pathway will have $s = -1/2$ (blue line). Strong repression is reflected by $s = -1$ (red line), whereas $s > 0$ correspond to synthetic interactions (purple line). **(B)** Epistasis plot showing that the *egl-9(lf); vhl-1(lf)* transcriptome deviates significantly from a null additive. Points are colored qualitatively according to density (purple—low, yellow—high) and size is inversely proportional to the standard error (S.E.) of the y-axis. The green line is the line of best fit from an orthogonal distance regression. **(C)** Comparison of simulated epistatic coefficients against the observed coefficient. Green curve shows the bootstrapped observed transcriptome-wide epistasis coefficient for *egl-9* and *vhl-1*. Dashed green line shows the mean value of the data. Simulations use only the single mutant data to idealize what expression of the double mutant should look like. $a > b$ means that the phenotype of a is observed in a double mutant $a^- b^-$.

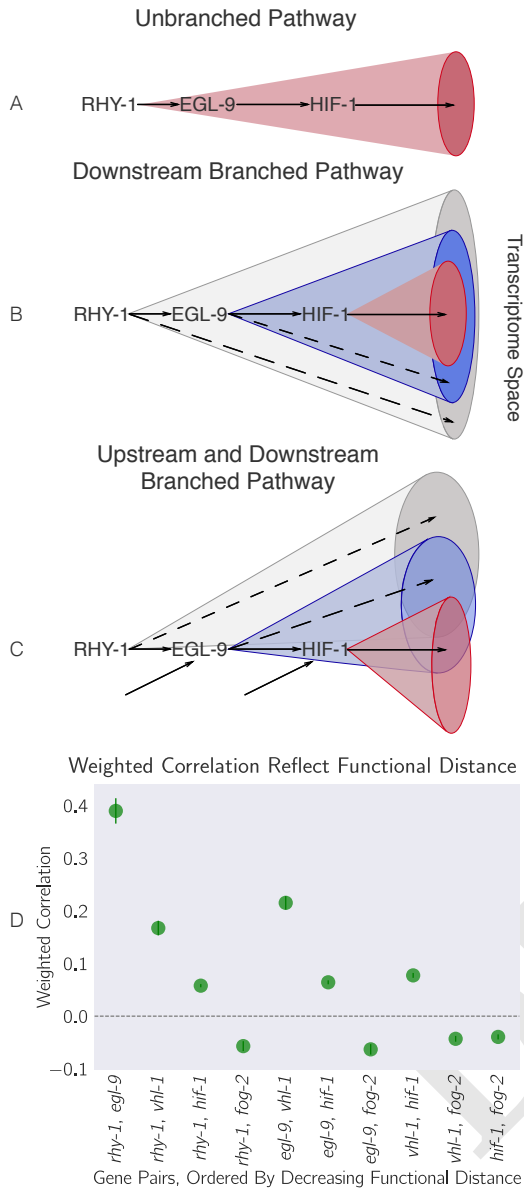


Fig. 6. Transcriptomes can be used to order genes in a pathway under certain assumptions. Arrows in the diagrams above are intended to show the direction of flow, and do not indicate valence. **A.** A linear pathway in which *rhy-1* is the only gene controlling *egl-9*, which in turn controls *hif-1* does not contain information to infer the order between genes. **B.** If *rhy-1* and *egl-9* have transcriptomic effects that are separable from *hif-1*, then the *rhy-1* transcriptome should contain contributions from *egl-9*, *hif-1* and *egl-9*- and *hif-1*-independent pathways. This pathway contains enough information to infer order. **C.** If a pathway is branched both upstream and downstream, transcriptomes will show even faster decorrelation. Nodes that are separated by many edges may begin to behave almost independently of each other with marginal transcriptomic overlap or correlation. **D.** The hypoxia pathway can be ordered. We hypothesize the rapid decay in correlation is due to a mixture of upstream and downstream branching that happens along this pathway. Bars show the standard error of the weighted coefficient from the Monte Carlo Markov Chain computations.

dynamics to infer gene order in a branching pathway, as we have done with the hypoxia pathway.

Classical epistasis identifies a core hypoxic response. We identified a main hypoxia response induced by HIF-1 (466 genes) by selecting genes that were consistently altered in *egl-9(lf)*, *rhy-1(lf)*, *vgl-1(lf)* and *egl-9(lf); vgl-1(lf)* mutants but which were suppressed in the *egl-9(lf) hif-1(lf)* mutant. This response included five transcription factors (*W02D7.6*, *nhr-57*, *ztf-18*, *nhr-135* and *dmd-9*; Supplementary Table 1). Even though HIF-1 is an activator, not all of these genes were up-regulated. We reasoned that only genes that are up-regulated in HIF-1-inhibitor mutants are candidates for direct regulation by HIF-1. We found 264 such genes. Phenotype Enrichment Analysis (27) showed that this gene list was enriched in genes associated with oxygen response, dauer development and dauer constitutive phenotypes (fold-change > 4; $q < 10^{-1}$ for all terms; see [Enrichment Analysis Notebook](#)).

Feedback can be inferred. While some of the rank plots contained a clear positive correlation (see Fig. 4), others showed a discernible cross-pattern (see Figure S2). In particular, this cross-pattern emerged between *vgl-1(lf)* and *rhy-1(lf)* or between *vgl-1(lf)* and *egl-9(lf)*, even though *vgl-1*, *rhy-1* and *egl-9* are all inhibitors of *hif-1(lf)*. Such cross-patterns could be indicative of feedback loops or other complex interaction patterns. If the above is correct, then it should be possible to identify genes that are regulated by *rhy-1* in a logically consistent way: Since loss of *egl-9* causes *rhy-1* mRNA levels to increase, if this increase leads to a significant change in RHY-1 activity, then it follows that the *egl-9(lf)* and *rhy-1(lf)* should show anti-correlation in a subset of genes. Since we do not observe many genes that are anti-correlated, we conclude that is unlikely that the change in *rhy-1* mRNA expression causes a significant change in RHY-1 activity under normoxic conditions. We also searched for genes with *hif-1*-independent, *vgl-1*-dependent gene expression and found 71 genes (Supplementary Table 2).

Identification of non-classical epistatic interactions. *hif-1(lf)* has traditionally been viewed as existing in a genetic OFF state under normoxic conditions. However, our dataset indicates that 1,075 genes show altered expression when *hif-1* function is removed in normoxic conditions. Moreover, we observed positive correlations between *hif-1(lf)* β coefficients and *egl-9(lf)*, *vgl-1(lf)* and *rhy-1(lf)* β coefficients in spite of the negative regulatory relationships between these genes and *hif-1*. Such positive correlations could indicate a relationship between these genes that has not been reported previously.

We identified genes that exhibited violations of the canonical genetic model of the hypoxia pathway (see [Non-canonical epistasis notebook](#)). We searched for genes that changed in different directions between *egl-9(lf)* and *vgl-1(lf)*, or, equivalently, between *rhy-1(lf)* and *vgl-1(lf)* (we assume that all results from the *rhy-1(lf)* transcriptome reflect a complete loss of *egl-9* activity) without specifying any further conditions. We found 56 that satisfied this condition (see Fig. 7, Supplementary Table 4). When we checked expression of these genes in the double mutant, we found that *egl-9* remained epistatic over *vgl-1* for this class of genes. This class of genes may in fact be much larger because it overlooks genes that have wild-type expression in an *egl-9(lf)* background, altered expression in a

396 *vhl-1(lf)* background, and suppressed (wild-type) expression in
397 an *egl-9(lf); vhl-1(lf)* background.

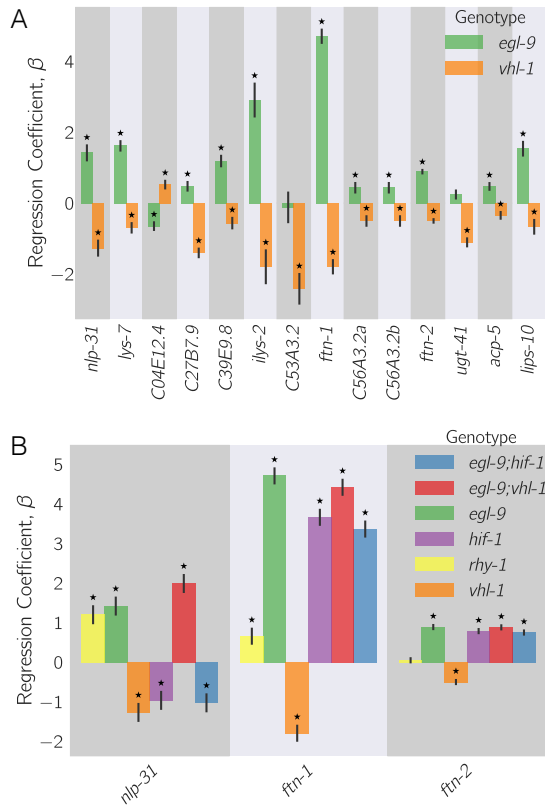


Fig. 7. A. 56 genes in *C. elegans* exhibit non-classical epistasis in the hypoxia pathway, characterized by opposite effects on gene expression, relative to the wild type, of the *vhl-1(lf)* compared to *egl-9(lf)* (or *rhy-1(lf)*) mutants. Shown are a random selection of 15 out of 56 genes for illustrative purposes. **B.** Genes that behave non-canonically have a consistent pattern. *vhl-1(lf)* mutants have an opposite effect to *egl-9(lf)*, but *egl-9* remains epistatic to *vhl-1* and loss-of-function mutations in *hif-1* suppress the *egl-9(lf)* phenotype. Asterisks show β values significantly different from 0 relative to wild type ($q < 10^{-1}$).

398 Although this entire class had similar behavior, we focused
399 on two genes, *nlp-31* and *ftn-1* which have representative
400 expression patterns. *ftn-1* is described to be responsive to
401 mutations in the hypoxia pathway and has been reported to
402 have aberrant behaviors; specifically, loss of function of *egl-9*
403 and *vhl-1* have opposing effects on *ftn-1* expression (28, 29).
404 These studies showed the same *ftn-1* expression phenotypes
405 using RNAi and alleles, allaying concerns of strain-specific
406 interference. We observed that *hif-1* was epistatic to *egl-9*,
407 and that *egl-9* and *hif-1* both promoted *ftn-1* expression.

408 Analysis of *ftn-1* expression reveals that *egl-9* is epistatic
409 to *hif-1*; that *vhl-1* has opposite effects to *egl-9*, and that
410 *vhl-1* is epistatic to *egl-9*. Analysis of *nlp-31* reveals similar
411 relationships. *nlp-31* expression is decreased in *hif-1(lf)*, and
412 increased in *egl-9(lf)*. However, *egl-9* is epistatic to *hif-1*. Like
413 *ftn-1*, *vhl-1* has the opposite effect to *egl-9*, yet is epistatic
414 to *egl-9*. We propose in the Discussion a novel model for how
415 HIF-1 might regulate these targets.

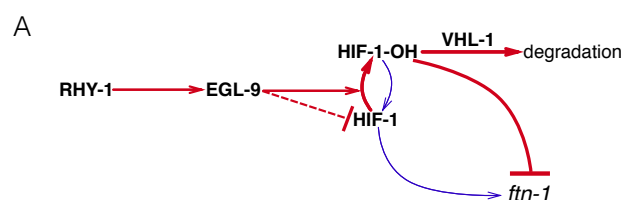
416 Discussion

417 **The *C. elegans* hypoxia pathway can be reconstructed de**
418 **novo from RNA-seq data.** We have shown that whole-organism

transcriptomic phenotypes can be used to reconstruct genetic
pathways and to discern previously uncharacterized genetic in-
teractions. We successfully reconstructed the hypoxia pathway
including the order of action of the genetic components and
its branching pattern. These results highlight the potential
of whole-animal expression profiles for dissecting molecular
pathways that are expressed in a large number of cells within
an organism. While our results are promising, it remains to be
seen whether our approach will also work for pathways that act
in a few cells. We selected a previously characterized pathway
because *C. elegans* is less amenable to high-throughput screens
compared to cultured cells. That said, the striking nature of
our results makes us optimistic that this technique could be
successfully used to reconstruct unknown pathways.

Interpretation of the non-classical epistasis in the hypoxia pathway. The 56 genes that exhibit a striking pattern of non-classical epistasis suggest the existence of previously undescribed aspects of the hypoxia pathway. Some of these non-classical behaviors had been observed previously (28–30), but no satisfactory mechanism has been proposed to explain them. Previous studies (28, 29) suggested that HIF-1 integrates information on iron concentration in the cell to determine its binding affinity to the *ftn-1* promoter, but could not definitively establish a mechanism. It is unclear why deletion of *hif-1* and deletion of *egl-9* both cause induction of *ftn-1* expression, but deletion of *vhl-1* abolishes this induction. Moreover, Luchachack et al (30) have previously reported that certain genes important for the *C. elegans* immune response against pathogens reflect similar non-canonical expression patterns. Their interpretation was that *swan-1*, which encodes a binding partner to EGL-9 (31), is important for modulating HIF-1 activity in some manner. The lack of a conclusive double mutant analysis in this work means the role of SWAN-1 in modulation of HIF-1 activity remains to be demonstrated. Other mechanisms, such as tissue-specific differences in the pathway (32) could also modulate expression, though it is worth pointing out that *ftn-1* expression appears restricted to a single tissue, the intestine (33). Another possibility is that *egl-9* controls *hif-1* mRNA stability via other *vhl-1*-independent pathways, but we did not see a decreases in *hif-1* level in *egl-9(lf)*, *rhy-1(lf)* or *vhl-1(lf)* mutants. Another possibility, such as control of protein stability via *egl-9* independently of *vhl-1* (34) will not lead to splitting unless it happens in a tissue-specific manner.

One parsimonious solution is to consider HIF-1 as a protein with both activating and inhibiting states. In fact, HIF-1 already exists in two states in *C. elegans*: unmodified HIF-1 and HIF-1-hydroxyl (HIF-1-OH). Under this model, the effects of HIF-1 for certain genes like *ftn-1* or *nlp-31* are antagonized by HIF-1-hydroxyl, which is present at only a low level in the cell in normoxia because it is degraded in a *vhl-1*-dependent fashion. This means that loss of *vhl-1* stabilizes HIF-1-hydroxyl. If *vhl-1* is inactivated, genes that are sensitive to HIF-1-hydroxyl will be inhibited as a result of the increase in HIF-1-hydroxyl, despite the increased levels of non-hydroxylated HIF-1. On the other hand, *egl-9(lf)* abrogates the generation of HIF-1-hydroxyl, stimulating accumulation of non-hydroxylated HIF-1 and promoting gene expression. Whether deletion of *hif-1(lf)* is overall activating or inhibiting will depend on the relative activity of each protein state under normoxia (see Fig. 8). HIF-1-hydroxyl is challenging to study genetically, and if it does have the activity suggested by our genetic evidence this



B

Genotype	Interpretation	
wild type	HIF-1 → ftn-1 HIF-1-OH	
<i>egl-9</i>	HIF-1 → ftn-1	HIF-1 activates/ HIF-1-OH represses
<i>vhl-1</i>	HIF-1 → ftn-1 HIF-1-OH	HIF-1-OH represses
<i>hif-1</i>	ftn-1	Depends on specific activities/ concentrations at S.S.
<i>egl-9; hif-1</i>	ftn-1	Depends on specific activities/ concentrations at S.S.
<i>egl-9; vhl-1</i>	HIF-1 → ftn-1	HIF-1 activates/ HIF-1-OH represses

Fig. 8. A hypothetical model showing a mechanism where HIF-1-hydroxyl antagonizes HIF-1 in normoxia. **A.** Diagram showing that RHY-1 activates EGL-9. EGL-9 hydroxylates HIF-1 in an oxygen-dependent manner. HIF-1 is rapidly hydroxylated and the product, HIF-1-OH is rapidly degraded in a VHL-1-dependent fashion. EGL-9 can also inhibit HIF-1 in an oxygen-independent fashion. In our model, HIF-1 and HIF-1-OH have opposing effects on transcription. The width of the arrows represents rates in normoxic conditions. **B.** Table showing the effects of loss-of-function mutations on HIF-1 and HIF-1-OH activity, showing how this can potentially explain the *ftn-1* expression levels in each case. S.S = Steady-state.

may have prevented such a role from being detected. No mimetic mutations are known with which to study the pure hydroxylated HIF-1 species, and mutations in the Von Hippel-Lindau gene that stabilize the hydroxyl species also increase the quantity of non-hydroxylated HIF-1 by mass action.

Because HIF-1 is detected at low levels in cells under normoxic conditions (35), total HIF-1 protein levels are assumed to be so low as to be biologically inactive. However, our data show 1,075 genes change expression in response to loss of *hif-1* under normoxic conditions, which establishes that there is sufficient total HIF-1 protein to be biologically active. Our analyses also revealed that *hif-1(lf)* shares positive correlations with *egl-9(lf)*, *rhy-1(lf)* and *vhl-1(lf)*, and that each of these genotypes also shows a secondary negative rank-ordered expression correlation with each other.

A homeostatic argument can be made in favor of the activity of HIF-1-hydroxyl. The cell must continuously monitor multiple metabolite levels. The *hif-1*-dependent hypoxia response integrates information from O₂, α-ketoglutarate and iron concentrations in the cell. One way to integrate this information is by encoding it within the effective hydroxylation rate of HIF-1 by EGL-9. Then the dynamics in this system will evolve exclusively as a result of the total amount of HIF-1 in the cell. Such a system can be sensitive to fluctuations in the absolute concentration of HIF-1 (36). Since the absolute levels of HIF-1 are low in normoxic conditions, small fluctuations in protein copy-number can represent a large fold-change in HIF-1 levels. These fluctuations might not be problematic for genes that must be turned on only under conditions of severe hypoxia—presumably, these genes would be activated only when HIF-1 levels increase far beyond random fluctuations.

For yet other sets of genes that must change expression in re-

sponse to the hypoxia pathway, it may not be sufficient to integrate metabolite information exclusively via EGL-9-dependent hydroxylation of HIF-1. In particular, genes that may function to increase survival in mild hypoxia may benefit from regulatory mechanisms that can sense minor changes in environmental conditions and which therefore benefit from robustness to transient changes in protein copy number. Likewise, genes that are involved in iron or α-ketoglutarate metabolism (such as *ftn-1*) may benefit from being able to sense, accurately, small and consistent deviations from basal concentrations of these metabolites. For these genes, the information may be better encoded by using HIF-1 and HIF-1-hydroxyl as an activator/repressor pair. Such circuits are known to possess distinct advantages for controlling output robustly to transient fluctuations in the levels of their components (37, 38).

Our RNA-seq data suggests that one of these atypical targets of HIF-1 may be RHY-1. Although *rhy-1* does not exhibit non-classical epistasis, all genotypes containing a *hif-1(lf)* mutation had increased expression levels of *rhy-1*. We speculate that if *rhy-1* is controlled by both HIF-1 and HIF-1-hydroxyl, then this might imply that HIF-1 auto-regulates both positively and negatively.

Strengths and weaknesses of the methodology. We have described a set of methods that can in principle be applied to any multidimensional phenotype. Although we have not applied these methods to *de novo* pathway discovery, we believe that they will be broadly applicable to a wide variety of genetic problems. One aspect of our methodology is the use of whole-organism expression data. Data collection from whole-organisms can be rapid with low technical barriers. On the other hand, a concern is that whole-organism data will average signals across tissues, which would limit the scope of this technology to the study of genetic pathways that are systemic or expressed in large tissues. In reality, our method may be applicable for pathways that are expressed even in a small number of cells in an organism. If a pathway is active in a single cell, this does not mean that it does not have cell-non-autonomous effects that could be detected on an organism-wide level. Thus, pathways that act in single cells could still be characterized via whole-organism transcriptome profiling. If the non-autonomous effects are long-lasting, then the profiling could take place after the time-of-action of this pathway. In fact, this is how the female-like state in *C. elegans* was recently identified (15): *fog-2* is involved in translation repression of *tra-2* in the somatic gonad, thereby promoting sperm formation in late larvae (39). Loss of this gene causes non-cell-autonomous effects that can be detected well after the time-of-action of *fog-2* in the somatic gonad has ended. Therefore, we believe that our methodology will be applicable to many genetic cases, with the exception of pathways that acts in complex, antagonistic manners depending on the cell type, or if the pathway minimally affects gene expression.

Genetic analysis of transcriptomic data has proved challenging as a result of its complexity. Although dimensionality reduction techniques such as PCA have emerged as powerful methods with which to understand these data, these methods generate reduced coordinates which are difficult or impossible to interpret. As an example, the first principal component in this paper (see Fig. 3) could be interpreted as HIF-1 pseudo-abundance (40). However, another equally reasonable, yet potentially completely different interpretation, is as a pseudo-

HIF-1/HIF-1-OH ratio. Another way to analyze genetic interactions is via general linear models (GLMs) that include interaction terms between two or more genes. GLMs can quantify the genetic interactions on single transcripts. We and others (14, 15) have used GLMs to perform epistasis analyses of pathways using transcriptomic phenotypes. GLMs are powerful, but they generate a different interaction coefficient for each gene measured. The large number of coefficients makes interpretation of the genetic interaction between two mutants difficult. Previous approaches (14) visualize these coefficients via clustered heatmaps. However, two clusters cannot be assumed to be evidence that two genes interact via entirely distinct pathways. Indeed, the non-classical epistasis examples we described here might cluster separately even though a reasonable model can be invoked that does not require any new molecular players.

The epistasis plots shown here are a useful way to visualize epistasis in vectorial phenotypes. We have shown how an epistasis plot can be used to identify interactions between two genes by examining the transcriptional phenotypes of single and double mutants. Epistasis plots can accumulate an arbitrary number of points within them, possess a rich structure that can be visualized and have straightforward interpretations for special slope values. Epistasis plots and GLMs are not mutually exclusive. A GLM could be used to quantify epistasis interactions at single-transcript resolution, and the results then analyzed using an epistasis plot (for a non-genetic example, see (15)). A benefit of epistasis plots is that they enable the computation of a single, aggregate statistic that describes the ensemble behavior of a set of genes. This aggregate statistic is not enough to describe all possible behaviors in a system, but it can be used to establish whether the genes under study are part of a single pathway. In the case of the hypoxia pathway, phenotypes that are downstream of the hypoxia pathway should conform to the genetic equalities, $egl-9(lf) \ hif-1(lf) = hif-1(lf) \text{ AND } egl-9(lf)$; $vhl-1(lf) = egl-9(lf)$. Genes whose expression levels behave strangely, yet satisfy these equalities are downstream of the hypoxia pathway. These anomalous genes cannot be identified via the epistasis coefficient but the epistasis coefficient does provide a unifying framework with which to analyze them by constraining the space of plausible hypotheses.

Until relatively recently, the rapid generation and molecular characterization of null mutants was a major bottleneck for genetic analyses. Advances in genomic engineering mean that, for a number of organisms, production of mutants is now rapid and efficient. As mutants become easier to produce, biologists are realizing that phenotyping and characterizing the biological functions of individual genes is challenging. This is particularly true for whole organisms, where subtle phenotypes can go undetected for long periods of time. We have shown that whole-animal RNA-sequencing is a sensitive method that can be seamlessly incorporated with genetic analyses of epistasis.

Materials and Methods

Nematode strains and culture. Strains used were N2 (Bristol), JT307 *egl-9(sa307)*, CB5602 *vhl-1(ok161)*, ZG31 *hif-1(ia4)*, RB1297 *rhy-1(ok1402)*, CB6088 *egl-9(sa307) hif-1(ia4)*, CB6116 *egl-9(sa307);vhl-1(ok161)*. Lines were grown on standard nematode growth media Petri plates seeded with OP50 *E. coli* at 20°C (41).

RNA isolation. Lines were synchronized by harvesting eggs via sodium hypochlorite treatment and subsequently plating eggs on food. Worms were staged and based on the time after plating, vulva morphology and the absence of eggs. 30–50 non-gravid young adults were picked and placed in 100 μ L of TE pH 8.0 (Ambion AM9849) in 0.2 mL PCR tubes on ice. Worms were allowed to settle or spun down by centrifugation and \sim 80 μ L of supernatant removed before flash-freezing in liquid N_2 . These samples were digested with Recombinant Proteinase K PCR Grade (Roche Lot No. 03115 838001) for 15 min at 60° in the presence of 1% SDS and 1.25 μ L RNA Secure (Ambion AM7005). 5 volumes of Trizol (Tri-Reagent Zymo Research) were added to the RNA samples and treated with DNase I using Zymo Research Quick-RNA MicroPrep R1050. Samples were analyzed run on an Agilent 2100 BioAnalyzer (Agilent Technologies). Replicates were selected that had RNA integrity numbers equal to or greater than 9.0 and without bacterial ribosomal bands, except for the ZG31 mutant where one of three replicates had a RIN of 8.3.

Library preparation and sequencing. 10 ng of total RNA from each sample was reverse-transcribed into cDNA using the Clontech SMARTer Ultra Low Input RNA for Sequencing v3 kit (catalog #634848) in the SMARTSeq2 protocol (42). RNA was denatured at 70°C for 3 min in the presence of dNTPs, oligo dT primer and spiked-in quantitation standards (NIST/ERCC from Ambion, catalog #4456740). After chilling to 4°C, the first-strand reaction was assembled using a LNA TSO primer (42), and run at 42°C for 90 minutes, followed by denaturation at 70°C for 10 min. The first strand reaction was used as template for 13 cycles of PCR using the Clontech v3 kit. Reactions were purified with Ampure XP SPRI beads (catalog #A63880). After quantification using the Qubit High Sensitivity DNA assay, a 3 ng aliquot of the cDNA was run on the Agilent HS DNA chip to confirm the length distribution of the amplified fragments. The median value for the average cDNA lengths from all length distributions was 1,076 bp. Tagmentation of the full length cDNA was performed using the Illumina/Nextera DNA library prep kit (catalog #FC-121-1030). Following Qubit quantitation and Agilent BioAnalyzer profiling, the tagged libraries were sequenced on an Illumina HiSeq2500 machine in single read mode with a read length of 50 nt to a depth of 15 million reads per sample. Base calls were performed with RTA 1.13.48.0 followed by conversion to FASTQ with bcl2fastq 1.8.4.

Read alignment and differential expression analysis. We used Kallisto (43) to perform read pseudo-alignment and performed differential analysis using Sleuth (44). We fit a general linear model for an isoform t in sample i :

$$y_{t,i} = \beta_{t,0} + \beta_{t,genotype} \cdot X_{t,i} + \beta_{t,batch} \cdot Y_{t,i} + \epsilon_{t,i} \quad [1]$$

where $y_{t,i}$ was the logarithm transformed counts of isoform t in sample i ; $\beta_{t,genotype}$ and $\beta_{t,batch}$ were parameters of the model for the isoform t , and which could be interpreted as biased estimators of the log-fold change; $X_{t,i}$, $Y_{t,i}$ were indicator variables describing the experimental conditions of the isoform t in sample i ; and $\epsilon_{t,i}$ was the noise associated with a particular measurement. After fitting the general linear model, we tested isoforms for differential expression using the built-in Wald-test in Sleuth (44), which outputs a q -value that has been corrected for multiple hypothesis testing.

Genetic Analysis, Overview. The processed data were analyzed using Python 3.5. We used the Pandas, Matplotlib, Scipy, Seaborn, Sklearn, Networkx, PyMC3, and TEA libraries (45–52). Our analysis is available in Jupyter Notebooks (53). All code and processed data are available at <https://github.com/WormLabCaltech/mpsq> along with version-control information. Our Jupyter Notebook and interactive graphs for this project can be found at <https://wormlabcaltech.github.io/mpsq/>. Raw reads were deposited in the Short Read Archive under the study accession number SRP100886.

Weighted correlations. Correlations between mutants were calculated by identifying their STP. Transcripts were rank-ordered according to their regression coefficient, β . Regressions were performed using a Student-T distribution with the PyMC3 library (48) (`pm.glm.families.StudentT` in Python). If the correlations had an average value > 1 , the average correlation coefficient was set to 1.

Weights were calculated as the number of genes that were inliers divided by the number of DEGs present in either mutant.

Epistatic analysis. The epistasis coefficient between two null mutants a and b was calculated as:

$$s(a, b) = \frac{\beta_{a,b} - \beta_a - \beta_b}{\beta_a + \beta_b} \quad [2]$$

Null models for various epistatic relationships were generated by sampling the single mutants in an appropriate fashion. For example, to generate the distribution for two mutants that obey the epistatic relationship $a^- = a^-b^-$, we substituted $\beta_{a,b}$ with β_a and bootstrapped the result.

To select between theoretical models, we implemented an approximate Bayesian Odds Ratio. We defined a free-fit model, M_1 , that found the line of best fit for the data:

$$P(\alpha | M_1, D) \propto \prod_{(x_i, y_i, \sigma_i) \in D} \exp\left[-\frac{(y_i - \alpha \cdot x_i)^2}{2\sigma_i^2}\right] \cdot (1 + \alpha^2)^{-3/2}, \quad [3]$$

where α was the slope to be determined, x_i, y_i are the of each point, and σ_i was the standard error associated with the y -value. We used equation 3 to obtain the most likely slope given the data, D , via minimization (`scipy.optimize.minimize` in Python). Finally, we approximated the odds ratio as:

$$OR = \frac{P(D | \alpha^*, M_1) \cdot (2\pi)^{1/2} \sigma_{\alpha^*}}{P(D | M_i)}, \quad [4]$$

where α^* was the slope found after minimization, σ_{α^*} was the standard deviation of the parameter at the point α^* and $P(D | M_i)$ was the probability of the data given the parameter-free model, M_i .

Enrichment analysis. Tissue, Phenotype and Gene Ontology Enrichment Analysis were carried out using the WormBase Enrichment Suite for Python (27, 51).

ACKNOWLEDGMENTS. This work was supported by HHMI with whom PWS is an investigator and by the Millard and Muriel Jacobs Genetics and Genomics Laboratory at Caltech. Strains were provided by the CGC, which is funded by the NIH Office of Research Infrastructure Programs (P40 OD010440). We thank Hillel Schwartz, Erich Schwarz, Jonathan Liu, Han Wang and Porfirio Quintero for their advice throughout this project.

1. Huang LS, Sternberg PW (2006) Genetic dissection of developmental pathways. *WormBook: the online review of C. elegans biology* (1995):1–19.
2. Phillips PC (2008) Epistasis—the essential role of gene interactions in the structure and evolution of genetic systems. *Nat Rev Genet* 9(11):855–867.
3. Mortazavi A, Williams BA, McCue K, Schaeffer L, Wold B (2008) Mapping and quantifying mammalian transcriptomes by RNA-Seq. *Nature Methods* 5(7):621–628.
4. Schwarz EM, Kato M, Sternberg PW (2012) Functional transcriptomics of a migrating cell in *Caenorhabditis elegans*. *Proceedings of the National Academy of Sciences of the United States of America* 109(4):16246–51.
5. Van Wolfswinkel JC, Wagner DE, Reddien PW (2014) Single-cell analysis reveals functionally distinct classes within the planarian stem cell compartment. *Cell Stem Cell* 15(3):326–339.
6. Scimone ML, Kravarik KM, Lapan SW, Reddien PW (2014) Neoblast specialization in regeneration of the planarian *Schmidtea mediterranea*. *Stem Cell Reports* 3(2):339–352.
7. Brem RB, Yvert G, Clinton R, Kruglyak L (2002) Genetic Dissection of Transcriptional Regulation in Budding Yeast. *Science* 296(5568).
8. Schadt EE, et al. (2003) Genetics of gene expression surveyed in maize, mouse and man. *Nature* 422(6929):297–302.
9. Li Y, et al. (2006) Mapping Determinants of Gene Expression Plasticity by Genetical Genomics in *C. elegans*. *PLoS Genetics* 2(12):e222.
10. King EG, Sanderson BJ, McNeil CL, Long AD, Macdonald SJ (2014) Genetic Dissection of the *Drosophila melanogaster* Female Head Transcriptome Reveals Widespread Allelic Heterogeneity. *PLoS Genetics* 10(5):e1004322.
11. Hughes TR, et al. (2000) Functional Discovery via a Compendium of Expression Profiles. *Cell* 102(1):109–126.
12. Capaldi AP, et al. (2008) Structure and function of a transcriptional network activated by the MAPK Hog1. *Nature Genetics* 40(11):1300–1306.
13. Van Driessche N, et al. (2005) Epistasis analysis with global transcriptional phenotypes. *Nature genetics* 37(5):471–477.
14. Dixit A, et al. (2016) Perturb-Seq: Dissecting Molecular Circuits with Scalable Single-Cell RNA Profiling of Pooled Genetic Screens. *Cell* 167(7):1853–1866.e17.
15. Angeles-Albore D, et al. (2017) The *Caenorhabditis elegans* Female-Like State: Decoupling the Transcriptomic Effects of Aging and Sperm Status. *G3: Genes, Genomes, Genetics* 7(9).
16. Epstein ACR, et al. (2001) *C. elegans* EGL-9 and mammalian homologs define a family of dioxygenases that regulate HIF by prolyl hydroxylation. *Cell* 107(1):43–54.

17. Shen C, Shao Z, Powell-Coffman JA (2006) The *Caenorhabditis elegans rhy-1* Gene Inhibits HIF-1 Hypoxia-Inducible Factor Activity in a Negative Feedback Loop That Does Not Include *vhl-1*. *Genetics* 174(3):1205–1214.
18. Shao Z, Zhang Y, Powell-Coffman JA (2009) Two Distinct Roles for EGL-9 in the Regulation of HIF-1-mediated gene expression in *Caenorhabditis elegans*. *Genetics* 183(3):821–829.
19. Jiang H, Guo R, Powell-Coffman JA (2001) The *Caenorhabditis elegans hif-1* gene encodes a bHLH-PAS protein that is required for adaptation to hypoxia. *Proceedings of the National Academy of Sciences of the United States of America* 98(14):7916–7921.
20. Loenarz C, et al. (2011) The hypoxia-inducible transcription factor pathway regulates oxygen sensing in the simplest animal, *Trichoplax adhaerens*. *EMBO reports* 12(1):63–70.
21. Jiang BH, Rue E, Wang GL, Roe R, Semenza GL (1996) Dimerization, DNA binding, and transactivation properties of hypoxia-inducible factor 1. *The Journal of biological chemistry* 271(30):17771–17778.
22. Powell-Coffman JA, Bradfield CA, Wood WB (1998) *Caenorhabditis elegans* Orthologs of the Aryl Hydrocarbon Receptor and Its Heterodimerization Partner the Aryl Hydrocarbon Receptor Nuclear Translocator. *Proceedings of the National Academy of Sciences* 95(6):2844–2849.
23. Huang LE, Arany Z, Livingston DM, Franklin Bunn H (1996) Activation of hypoxia-inducible transcription factor depends primarily upon redox-sensitive stabilization of its alpha subunit. *Journal of Biological Chemistry* 271(50):32253–32259.
24. Kaelin WG, Ratcliffe PJ (2008) Oxygen Sensing by Metazoans: The Central Role of the HIF Hydroxylase Pathway. *Molecular Cell* 30(4):393–402.
25. Ma DK, Vozdek R, Bhatla N, Horvitz HR (2012) CYSL-1 Interacts with the O 2-Sensing Hydroxylase EGL-9 to Promote H 2S-Modulated Hypoxia-Induced Behavioral Plasticity in *C. elegans*. *Neuron* 73(5):925–940.
26. Yeung KY, Ruzzo WL (2001) Principal component analysis for clustering gene expression data. *Bioinformatics (Oxford, England)* 17(9):763–774.
27. Angeles-Albore D, Lee RY, Chan J, Sternberg PW (2017) Phenotype and gene ontology enrichment as guides for disease modeling in *C. elegans*. *bioRxiv*.
28. Ackerman D, Gens D (2012) Insulin/IGF-1 and hypoxia signaling act in concert to regulate iron homeostasis in *Caenorhabditis elegans*. *PLoS Genetics* 8(3).
29. Romney SJ, Newman BS, Thacker C, Leibold EA (2011) HIF-1 regulates iron homeostasis in *Caenorhabditis elegans* by activation and inhibition of genes involved in iron uptake and storage. *PLoS Genetics* 7(12).
30. Luhachack LG, et al. (2012) EGL-9 Controls *C. elegans* Host Defense Specificity through Prolyl Hydroxylation-Dependent and -Independent HIF-1 Pathways. *PLoS Pathogens* 8(7):48.
31. Shao Z, Zhang Y, Ye Q, Saldanha JN, Powell-Coffman JA (2010) *C. elegans swan-1* binds to *egl-9* and regulates *hif-1*-mediated resistance to the bacterial pathogen *Pseudomonas aeruginosa* PAO1. *PLoS Pathogens* 6(8):91–92.
32. Budde MW, Roth MB (2010) Hydrogen Sulfide Increases Hypoxia-inducible Factor-1 Activity Independently of von Hippel-Lindau Tumor Suppressor-1 in *C. elegans*. *Molecular biology of the cell* 21:212–217.
33. Kim YI, Cho JH, Yoo OJ, Ahnn J (2004) Transcriptional Regulation and Life-span Modulation of Cytosolic Aconitase and Ferritin Genes in *C. elegans*. *Journal of Molecular Biology* 342(2):421–433.
34. Chintala S, et al. (2012) Prolyl hydroxylase 2 dependent and Von-Hippel-Lindau independent degradation of Hypoxia-inducible factor 1 and 2 alpha by selenium in clear cell renal cell carcinoma leads to tumor growth inhibition. *BMC Cancer* 12(1):293.
35. Wang GL, Semenza GL (1993) Characterization of hypoxia-inducible factor 1 and regulation of DNA binding activity by hypoxia. *The Journal of biological chemistry* 268(29):21513–8.
36. Goentoro L, Shoval O, Kirschner MW, Alon U (2009) The Incoherent Feedforward Loop Can Provide Fold-Change Detection in Gene Regulation. *Molecular Cell* 36(5):894–899.
37. Hart Y, Antebi YE, Mayo AE, Friedman N, Alon U (2012) Design principles of cell circuits with paradoxical components. *Proceedings of the National Academy of Sciences of the United States of America* 109(21):8346–8351.
38. Hart Y, Alon U (2013) The Utility of Paradoxical Components in Biological Circuits. *Molecular Cell* 49(2):213–221.
39. Clifford R, et al. (2000) FOG-2, a novel F-box containing protein, associates with the GLD-1 RNA binding protein and directs male sex determination in the *C. elegans* hermaphrodite germline. *Development (Cambridge, England)* 127(24):5265–5276.
40. Lönnberg T, et al. (2017) Single-cell RNA-seq and computational analysis using temporal mixture modeling resolves TH1/TFH fate bifurcation in malaria. *Science Immunology* 2(9).
41. Sulston JE, Brenner S (1974) The DNA of *Caenorhabditis elegans*. *Genetics* 77(1):95–104.
42. Picelli S, et al. (2014) Full-length RNA-seq from single cells using Smart-seq2. *Nature protocols* 9(1):171–81.
43. Bray NL, Pimentel HJ, Melsted P, Pachter L (2016) Near-optimal probabilistic RNA-seq quantification. *Nature biotechnology* 34(5):525–7.
44. Pimentel HJ, Bray NL, Puente S, Melsted P, Pachter L (2016) Differential analysis of RNA-Seq incorporating quantification uncertainty. *bioRxiv* p. 058164.
45. McKinney W (2011) pandas: a Foundational Python Library for Data Analysis and Statistics. *Python for High Performance and Scientific Computing* pp. 1–9.
46. Oliphant TE (2007) SciPy: Open source scientific tools for Python. *Computing in Science and Engineering* 9:10–20.
47. Pedregosa F, et al. (2012) Scikit-learn: Machine Learning in Python. *Journal of Machine Learning Research* 12:2825–2830.
48. Salvatier J, Wiecki T, Fonnesbeck C (2015) Probabilistic Programming in Python using PyMC. *PeerJ Computer Science* 2(e55):1–24.
49. Van Der Walt S, Colbert SC, Varoquaux G (2011) The NumPy array: A structure for efficient numerical computation. *Computing in Science and Engineering* 13(2):22–30.
50. Hunter JD (2007) Matplotlib: A 2D graphics environment. *Computing in Science and Engineering* 9(3):99–104.
51. Angeles-Albore D, N. Lee RY, Chan J, Sternberg PW (2016) Tissue enrichment analysis for *C. elegans* genomics. *BMC Bioinformatics* 17(1):366.
52. Waskom M, et al. (2016) seaborn: v0.7.0 (January 2016).

850 53. Pérez F, Granger B (2007) IPython: A System for Interactive Scientific Computing Python: An
851 Open and General- Purpose Environment. *Computing in Science and Engineering* 9(3):21–
852 29.

DRAFT